Received: 28 September 2021 | Revised: 20 November 2021 | Accepted: 24 December 2021

DOI: 10.1002/jbio.202100301

RESEARCH ARTICLE

JOURNAL OF BIOPHOTONICS

Investigation of nonlinear photoacoustic microscopy using a low-cost infrared lamp

Myeongsu Seong[1,2,3] | **Wenzhao Yang**[3] | **Yujie Han**[4] | **Jiasheng Zhou**[3] | **Lili Jing**[4] | **Sung-Liang Chen**[3,5,6*]

[1]School of Information Science and Technology, Nantong University, Nantong, Jiangsu, China

[2]Research Center for Intelligent Information Technology, Nantong University, Nantong, Jiangsu, China

[3]University of Michigan-Shanghai Jiao Tong University Joint Institute, Shanghai Jiao Tong University, Shanghai, China

[4]School of Pharmacy, Shanghai Jiao Tong University, Shanghai, China

[5]Engineering Research Center of Digital Medicine and Clinical Translation, Ministry of Education, Shanghai, China

[6]State Key Laboratory of Advanced Optical Communication Systems and Networks, Shanghai Jiao Tong University, Shanghai, China

***Correspondence**
Sung-Liang Chen, University of Michigan-Shanghai Jiao Tong University Joint Institute, Shanghai Jiao Tong University, Shanghai 200240, China.
Email: sungliang.chen@sjtu.edu.cn

Funding information
National Natural Science Foundation of China (NSFC), Grant/Award Number: 61775134

Abstract

Nonlinear photoacoustic microscopy (PAM) is a novel approach to enhance contrast and resolution. In this study, a low-cost infrared (IR) lamp as a simple approach for nonlinear PAM is demonstrated. Numerical simulations are first performed to verify the nonlinear photoacoustic effect under steady heating for two cases: (a) Differentiation of absorbers with different Grüneisen coefficients; (b) enhancement of photoacoustic amplitude. Then, sets of experiments are conducted to experimentally demonstrate our proposed approach: (a) Longitudinal monitoring of photoacoustic A-line signals from two samples, porcine tissue ex vivo and hemoglobin and indocyanine green (ICG) solutions in tubes in vitro for demonstrating the above-mentioned two cases; (b) PAM imaging of hemoglobin and ICG solutions in tubes before and after IR lamp heating. Different signal change and amplitude enhancement are observed in different demonstrations, showing the efficacy of the proposed approach. By virtue of cost-effectiveness and decent performance, our work facilitates nonlinear PAM studies.

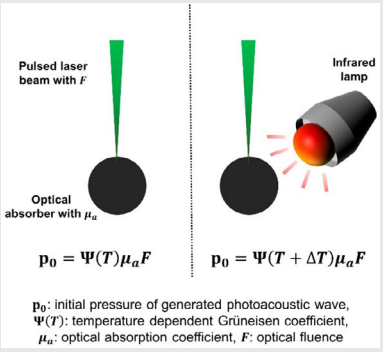

KEYWORDS

infrared heating, infrared lamp, low-cost, nonlinear photoacoustic effect, photoacoustic imaging, photoacoustic microscopy

1 | INTRODUCTION

Photoacoustic imaging (PAI) is based on the detection of acoustic waves generated by light illumination of an absorber and the consequent thermoelastic expansion. It has drawn increasing popularity due to its capability of visualizing structural and functional information of biological samples with scalable imaging depth and resolution [1, 2]. PAI has various implementations including

Abbreviations: 1D, one-dimensional; 2D, two-dimensional; 3D, three-dimensional; AR-PAM, acoustic-resolution photoacoustic microscopy; GR-PAM, Grüneisen relaxation photoacoustic microscopy; HIFU, high-intensity focused ultrasound; ICG, indocyanine green; IR, infrared; MAP, maximum amplitude projection; OR-PAM, optical-resolution photoacoustic microscopy; PAI, photoacoustic imaging; PAM, photoacoustic microscopy; PRF, pulse repetition frequency; SHG, second harmonic generation; SMF, single-mode fiber; SNR, signal-to-noise ratio.

photoacoustic computed tomography, photoacoustic microscopy (PAM) and photoacoustic endoscopy [1, 2]. Among them, PAM is mainly known for high resolution, relatively shallow imaging depth and simplicity of image reconstruction. PAM is further classified into optical-resolution PAM (OR-PAM) and acoustic-resolution PAM (AR-PAM). OR-PAM uses a tightly focused optical beam, which determines the lateral resolution of OR-PAM, while AR-PAM typically employs a focused acoustic transducer to provide the lateral resolution of AR-PAM [1–3]. Using PAM, various endogenous and exogenous chromophores can be visualized with high resolution by light illumination with proper optical wavelengths.

Recently, nonlinear PAM has been extensively explored as an approach to improve resolution and image contrast of PAM. For example, Grüneisen relaxation PAM (GR-PAM) utilized two laser pulses that have a time interval shorter than sub-microseconds [4]. GR-PAM moderately improved lateral resolution and dramatically improved axial resolution, enhancing the depth-resolved ability in PAI. GR-PAM for in vivo imaging of the mouse brain, label-free cell nucleus and lipid-rich porcine tissue was also demonstrated [5–7]. Another study showed contrast enhancement by utilizing heat accumulation caused by multiple pulse trains with pulse intervals shorter than the thermal relaxation time [8]. Contrast enhancement was demonstrated for both phantoms and contrast agents injected under the abdominal layer of a rat. Another work introduced a thermal contrast parameter to emphasize the contrast enhancement due to heating, and ex vivo imaging of porcine tissue was demonstrated [9]. Besides, by employing a combination of a set of continuous-wave lasers with different wavelengths (for heating) and a pulsed laser (for photoacoustic excitation), selective contrast enhancement of different absorbers was achieved [10]. Another recent work proposed using a continuous-wave laser for heating an absorber [11]. This work demonstrated enhancement of photoacoustic amplitude of multiple samples using the continuous-wave laser with a wavelength corresponding to the high absorption wavelength of the samples. Photoacoustic phasoscopy was introduced to greatly improve the contrast of photoacoustic images by utilizing both light scattering signals and detected photoacoustic signals [12]. There were a few studies based on nonlinear optics such as multiphoton excitation and second harmonic generation (SHG) for photoacoustic resolution and contrast enhancement [13, 14].

While the above works are effective, several aspects may limit the wide applications of nonlinear PAM. First, additional laser sources are required, imposing high cost on the imaging system [4–6, 10]. Secondly, sophisticated control of the time intervals between laser pulses (e.g., a time interval shorter than the thermal relaxation time of a medium of interest) makes the experimental implementation complicated [4–10, 14]. The mechanism is termed transient heating, in contrast to steady heating [15–17]. Thirdly, depending on the absorption spectrum of a sample, continuous-wave lasers with different wavelengths or a tunable laser is required to effectively modulate the temperature [11], which also increases the cost and/or complexity of the system. While photoacoustic phasoscopy enhances image contrast dramatically, it cannot be applied to deep samples due to strong light scattering at depth [12]. SHG-based PAI sacrifices axial resolution and multiphoton excitation for PAI uses high power illumination, which may cause irreversible photodamage [13, 14].

Here, we introduce a low-cost and simple approach for nonlinear PAM using an infrared (IR) lamp for steady heating. To validate the feasibility and versatility of the proposed scheme, a set of simulations were performed assuming two cases: contrast enhancement of absorbers with different Grüneisen coefficients and enhancement of photoacoustic amplitude. Then, a variety of samples including porcine tissue and the tubes containing hemoglobin and indocyanine green (ICG) solutions were studied ex vivo and in vitro, respectively. The results show that our nonlinear PAM technique applies to these samples to enhance contrast (for the case of porcine tissue) and signal-to-noise ratio (SNR) (for the case of tube samples). The contributions of this work include: (a) We propose a new approach for low-cost and simple nonlinear PAM using an IR lamp; (b) our approach can be used to enhance contrast of absorbers and SNR depending on samples; (c) we further demonstrate the feasibility and potential of enhancing SNR of our approach for in vitro nonlinear PAM imaging. In addition, our approach does not lose several advantages of PAM, including decent penetration and three-dimensional (3D) imaging, although not explicitly demonstrated in this work.

2 | METHODS

2.1 | Theory and simulation

In PAI, the initial pressure of generated photoacoustic waves can be simply described as,

$$p_0 = \Psi(T)\mu_a F, \tag{1}$$

where Ψ is the unitless temperature-dependent Grüneisen coefficient, T is the temperature, μ_a is the absorption coefficient of an absorber and F is the fluence of illumination [1–3]. The Grüneisen coefficient, Ψ, is further expressed as $\Psi = \beta v_s^2 / C_p$, where β is the thermal

expansion coefficient, v_s is the speed of sound and C_p is the specific heat [2, 18, 19]. In general, all of β, v_s and C_p are temperature-dependent, too. As the temperature of the absorber and/or its surrounding medium changes, the Grüneisen coefficient changes, which, in turn, results in change in photoacoustic amplitude (p_0). As a result, the simple linear relation between p_0 and F no longer holds as temperature changes, which is called nonlinear photoacoustic effect. Note that here μ_a is assumed to be constant.

In this study, a low-cost IR lamp was used to alter the temperature of the absorber and the medium. By modulating temperature using an IR lamp, depending on the characteristics of absorbers, contrast enhancement of absorbers with different thermoacoustic properties and enhancement of photoacoustic amplitude are possible. To be specific, assuming T_0 is the baseline temperature (before heating), T_1 is the temperature after heating. Grüneisen coefficient of one absorber is denoted as Ψ_a, and that of the other absorber is Ψ_b. The change of Grüneisen coefficient of the first absorber is denoted as $\Delta\Psi_a = \Psi_a(T_1) - \Psi_a(T_0)$, and that of the second absorber is $\Delta\Psi_b = \Psi_b(T_1) - \Psi_b(T_0)$. When $\Delta\Psi_a \neq \Delta\Psi_b$ (i.e., two absorbers having different change of the temperature-dependent Grüneisen coefficient $\Psi(T)$ before and after heating; e.g., described later in Figure 1), the proposed approach can be utilized to enhance contrast between the two absorbers. By contrast, when $\Delta\Psi_a \cong \Delta\Psi_b$ (i.e., two absorbers having the same or similar temperature-dependent Grüneisen coefficient $\Psi(T)$ before and after heating; e.g., described later in Figure 2), the two absorbers cannot be distinguished by our approach. Fortunately, given $\Delta\Psi_a > 0$ and $\Delta\Psi_b > 0$, our approach can still be used to enhance photoacoustic amplitude of the first and the second absorbers, respectively.

To better illustrate the two cases via nonlinear photoacoustic effect, numerical simulation was performed using k-wave toolbox [20]. To firstly demonstrate contrast enhancement, properties of porcine tissue were assumed. As temperature rises, porcine muscle shows increase of Grüneisen coefficient while porcine fat shows decrease of Grüneisen coefficient [9]. The parameters used in this simulation are as follows. (a) Absorption coefficients, μ_a: Due to the unavailability of optical properties of porcine tissue at wavelength of 532 nm (the illumination wavelength used in the study), we used the wavelength-averaged (430–

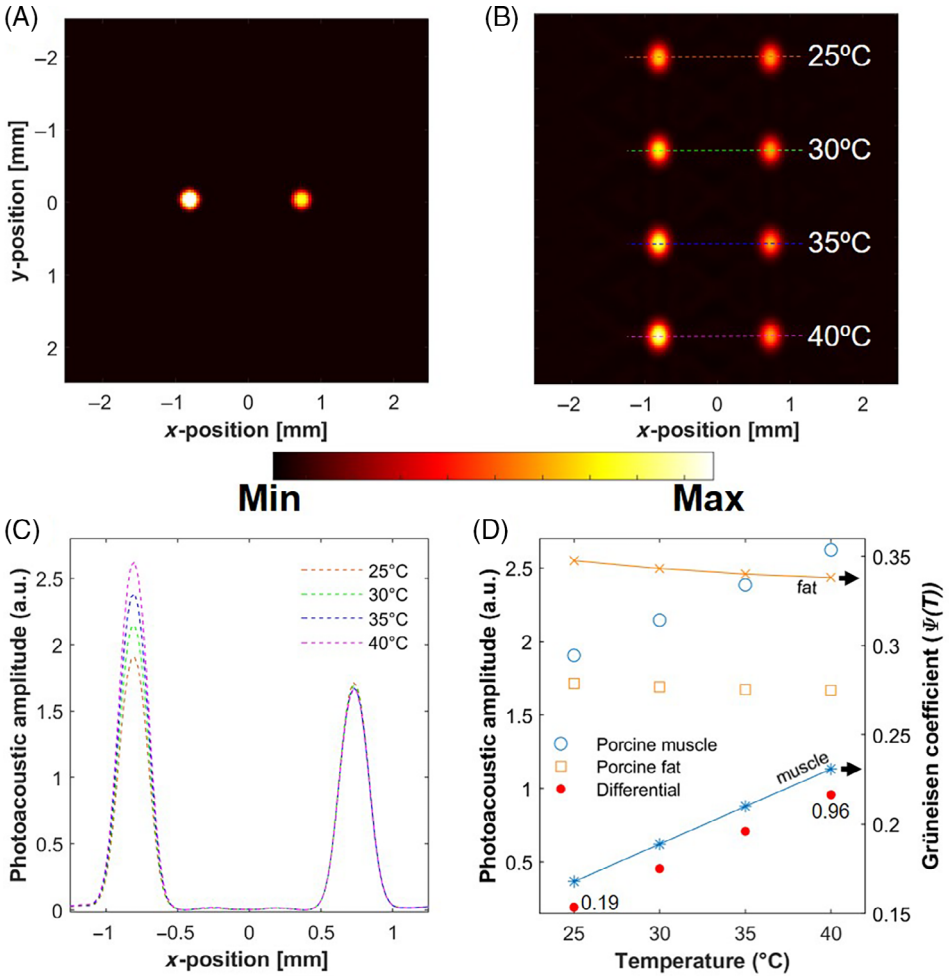

FIGURE 1 Illustration of contrast enhancement between two absorbers with different trends of Grüneisen coefficient via nonlinear photoacoustic effect. (A) Simulated photoacoustic image of porcine muscle (left) and fat (right). (B) Simulated photoacoustic image as temperature rises for the two samples: muscle (left) and fat (right). (C) The 1D profiles of photoacoustic amplitude along the lines indicated in (B) as temperature rises. (D) Peak photoacoustic amplitude in (C) as temperature rises for porcine muscle and fat. Blue (muscle) and orange (fat) lines indicate the variation of the Grüneisen coefficient as a function of temperature. Red dots indicate differential photoacoustic amplitude

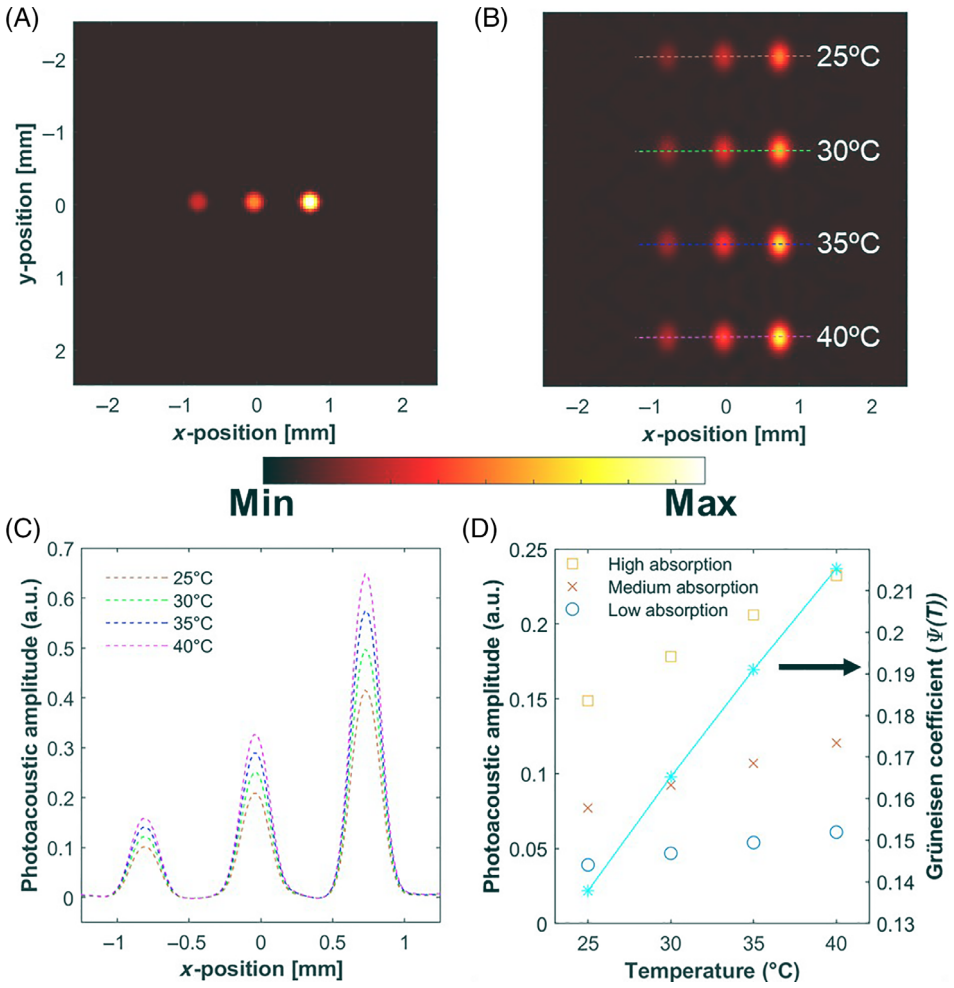

FIGURE 2 Illustration of enhancement of photoacoustic amplitude as temperature changes. (A) Simulated photoacoustic image of the three absorbers with different absorption coefficients (μ_a ratio = 1:2:4 from left to right). (B) Simulated photoacoustic image as temperature rises for the three absorbers: μ_a ratio = 1:2:4 from left to right. (C) The 1D profiles of photoacoustic amplitude along the lines indicated in (B) as temperature rises. (D) Peak photoacoustic amplitude in (C) as temperature rises for the three absorbers. A cyan line indicates the variation of the Grüneisen coefficient as a function of temperature. For simplicity, this variation is assumed to be the same for the three absorbers

630 nm) optical properties of porcine tissue [21–25]. The absorption coefficient of porcine muscle of ~0.78 cm^{-1} was used [21]. It is known that porcine fat usually consists of 22% of water and 78% of pure fat [22], and thus, we calculated the absorption coefficient of porcine fat to be ~0.02 cm^{-1} based on the percentage of water and pure porcine fat and their absorption coefficients [22–25]. (b) Thermoacoustic parameters, including the thermal expansion coefficient, β, the speed of sound, v_s and the specific heat, C_p: Due to the unavailable thermoacoustic parameters of porcine tissue, those of bovine tissue were used instead [18, 22, 26–29]. (c) Illumination fluence, F: the fluence was set to a constant of 1 (i.e., $F = 1$ in Equation (1)). The temperature was varied from 25°C to 40°C with an increment of 5°C. Figure 1A shows the photoacoustic image (distribution of photoacoustic amplitude) of two absorbers with the photoacoustic characteristics of porcine muscle and fat. Figure 1B,C shows the change of photoacoustic image and one-dimensional (1D) profiles of photoacoustic amplitude along the lines indicated in Figure 1B as temperature rises, respectively. Figure 1D shows the peak photoacoustic amplitude, the differential photoacoustic amplitude (defined as (peak photoacoustic amplitude of porcine muscle) − (peak photoacoustic amplitude of porcine fat)) and Grüneisen coefficient of porcine muscle and fat as temperature changes. In Figure 1D, due to the different change of Grüneisen coefficients caused by temperature elevation, as temperature increases, the photoacoustic amplitude of porcine muscle also increases while that of porcine fat slightly decreases. The differential photoacoustic amplitude is from 0.19 to 0.96 as temperature increases from 25°C to 40°C (about five times enhancement). As a consequence, this simulation confirmed the feasibility of enhancing photoacoustic contrast of two different absorbers by modulating the temperature via steady heating. Note that F can be set to other constant values, and the conclusions of Figure 1 will remain the same.

In the second simulation, to demonstrate enhancement of photoacoustic amplitude, we assumed three samples with different absorption coefficients (the ratio of μ_a = 1:2:4, named low absorption, medium absorption and high absorption, respectively), constant fluence of 1 (i.e., $F = 1$ in Equation (1)) and for simplicity, the same

temperature-dependent Grüneisen coefficient $\Psi(T)$ (for convenience, β, v_s and C_p of water [30, 31] were assumed). The temperature was varied from 25°C to 40°C with an increment of 5°C. Note that the absorption coefficients were assumed to be fixed throughout the temperature variation. Figure 2A shows the photoacoustic image of the three absorbers. Figure 2B,C shows the change of photoacoustic image and 1D profiles of photoacoustic amplitude along the lines indicated in Figure 2B as temperature rises, respectively. Figure 2D shows the peak photoacoustic amplitude of the three absorbers and Grüneisen coefficient of the absorbers as temperature changes. As can be seen, for the three samples, photoacoustic amplitude increases as temperature rises because of the increase of Ψ with increased temperature.

$\Psi(T)$ is mainly associated with the thermoacoustic properties of the absorbers. From Equation (1), p_0 is linearly proportional to $\Psi(T)$. That is, to a first approximation, photoacoustic amplitude is linearly proportional to $\Psi(T)$. As can be seen in Figures 1D and 2D, the change of photoacoustic amplitude with temperature follows almost the same trends as the change of Grüneisen coefficient with temperature, $\Psi(T)$.

2.2 | IR lamp

A low-cost 100-W IR lamp (wavelength: ~0.6–2.5 μm; peak wavelength: ~1.1 μm; R95, Philips) with a controller, which costs ~$20 in total, was used to induce nonlinear variation of photoacoustic amplitude. The controller was used to set the illumination intensity and period of the IR lamp. Although the controller has 30 levels to adjust the illumination intensity of the IR lamp with nominal temperature from 30°C to 60°C, in our experiment, temperature was measured by a thermistor. For AR-PAM measurements, the IR lamp was simply placed under a water tank to effectively deliver IR heating light to absorbers and water, as shown in Figure 3A. For OR-PAM measurements, the IR lamp combined with a home-made reflective light guide (using an aluminum foil) for more directed IR lamp heating was obliquely placed at the same side as the laser illumination probe (Figure 3B), which enables reflection-mode operation. It is worth noting that temperature modulation happens via increasing water temperature for both AR-PAM and OR-PAM. The stability of the IR lamp was confirmed by monitoring the temperature of the IR lamp for 30 minutes using a thermographic camera (Compact Pro, Seek Thermal) prior to experiments for nonlinear PAM.

2.3 | AR-PAM

An AR-PAM system was used for nonlinear PAM experiments, as shown in Figure 3A. It is similar to the system used in our previous work [32]. A 6 ns pulsed laser (Q-smart 450, Quantel) with pulse repetition frequency (PRF) of 20 Hz and wavelength of 532 nm was used for photoacoustic excitation. The laser was coupled into a multimode optical patch cord (MHP910L02, Thorlabs). Then, a fiber aligner (LP-05A, Newport) with a

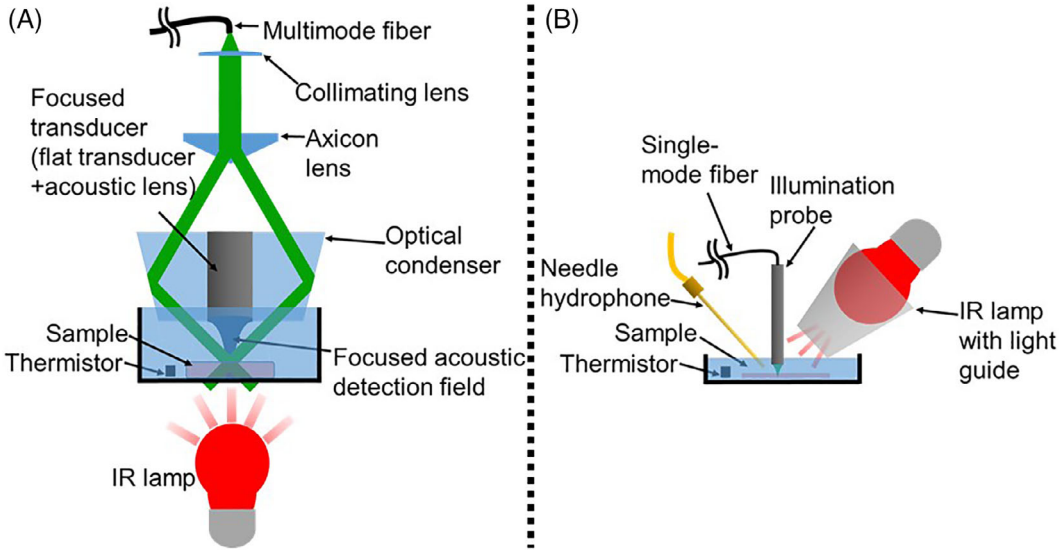

FIGURE 3 Schematic of AR-PAM (A) and OR-PAM (B) with IR lamp heating. The focused transducer in (A) is constructed by attaching an acoustic lens to a flat transducer

collimating lens (LA1540, Thorlabs) was used to collimate the laser beam. The collimated light was transformed to a semi-Bessel beam through an axicon lens (131-1240, EKSMA Optics). Finally, weakly-focused dark-field illumination was achieved by a custom-made acrylic optical condenser.

To acquire photoacoustic signals, a 50-MHz flat transducer (V214-BB-RM, −6 dB bandwidth: ~78%, Olympus) with an acoustic lens (45006, Edmund Optics) attached was placed at the center of the optical condenser. During image acquisition, the imaging head of AR-PAM, consisting of the laser illumination parts and the acoustic detection parts, was fixed with a two-dimensional (2D) motorized stage (M-L01.2A1, Physik Instrumente) for 2D raster scanning. Detected photoacoustic signals were amplified by a low-noise preamplifier (ZFL-500LN+, Mini-Circuits) and recorded by an oscilloscope (HDO4024, Teledyne LeCroy). When the photoacoustic amplitude was too weak, for example, for porcine tissue (described later in Section 3.1), two pre-amplifiers (ZFL-500LN+) were cascaded to further amplify the signals while the overall noise was less enhanced, leading to net improvement of SNR. This scheme to boost SNR was also adopted previously [33]. The data were saved in a computer for display and post-processing. Lateral and axial resolutions of the AR-PAM system were measured to be approximately 65 and 40 μm, respectively [32]. A thermistor (10 MΩ), connected with an Arduino board (Arduino Uno, Arduino), was placed inside the water tank to monitor the temperature changes.

2.4 | OR-PAM

An OR-PAM system used in this work is shown in Figure 3B. A solid-state 532 nm pulsed laser (FDSS532-Q3, CryLas) with pulse duration of <2 ns and PRF of 1 kHz was used. The laser was coupled into a single-mode fiber (SMF) with cut-off wavelength of 1260 nm (SMF-28e, Corning) using a doublet (AC127-030-A-ML, Thorlabs). An illumination probe mainly consisting of the SMF and a plano-convex lens (43 397, Edmund Optics) was used to produce a focused laser beam [34, 35], which was used for photoacoustic excitation. The pulse energy was set to 300 nJ/pulse for measurements. A custom-made needle hydrophone (35 MHz central frequency) was used to acquire photoacoustic signals. Similarly, for image acquisition, the illumination probe and the needle hydrophone were fixed with a 2D motorized stage for scanning. The photoacoustic signals acquired by the hydrophone were pre-amplified, recorded by a digitizer (CSE1422, Gage) and then stored in a computer. Lateral resolution of the OR-PAM system was measured to be ~10 μm. The same thermistor (10 MΩ) mentioned above was used to track the temperature changes.

2.5 | Nonlinear photoacoustic effect through longitudinal monitoring

Longitudinal monitoring of nonlinear photoacoustic signals due to IR lamp heating was conducted on two samples using the AR-PAM system without raster scanning. The samples were immersed in water. The first sample, an excised porcine tissue including muscle and fat, was used to demonstrate photoacoustic contrast enhancement. As described in Section 2.1, numerical simulation of porcine tissue was also performed. The second sample, three capillary tubes containing hemoglobin solution (Hefei Bomei Biotech.), 10 mg/mL ICG (ICG, Cardiogreen Innochem) and 5 mg/mL ICG, was chosen to demonstrate the enhancement of photoacoustic amplitude and SNR. For the above measurements, we kept monitoring photoacoustic amplitude from the baseline temperature (before IR lamp heating) and during the temperature increase (after starting the IR lamp heating).

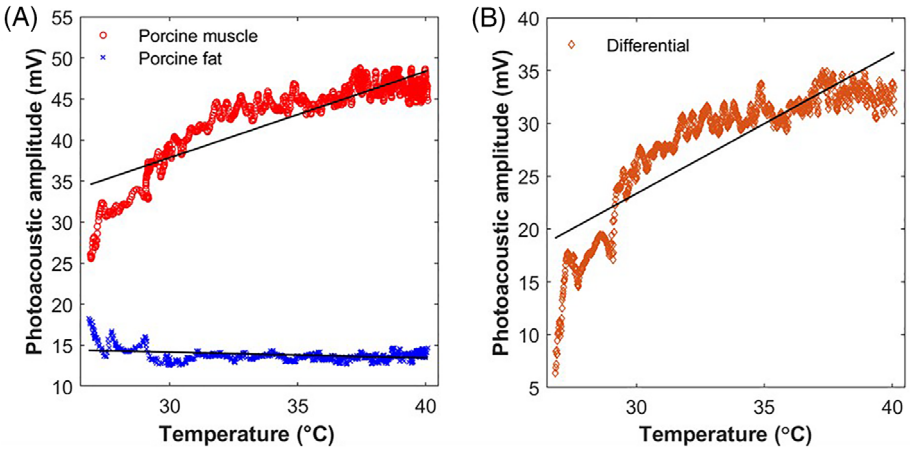

FIGURE 4 (A) Photoacoustic amplitude of porcine muscle and porcine fat as temperature rises. Photoacoustic amplitude of porcine tissue gradually increases while photoacoustic amplitude of porcine fat gradually decreases with temperature. (B) Differential photoacoustic amplitude as temperature rises. The differential photoacoustic amplitude increases from 6.4 (the minimum) to 34.9 mV (the maximum). Black lines are linear fits to experimental data

2.6 | In vitro imaging

To demonstrate the wide applicability of our approach for 2D imaging with different spatial resolution, raster scanning over the second sample mentioned above was performed using both AR-PAM and OR-PAM. Similarly, the tubes were immersed in water. Note that in OR-PAM, the hemoglobin solution was replaced with sheep blood for higher SNR. The PAM images before and after IR lamp heating were acquired for comparison.

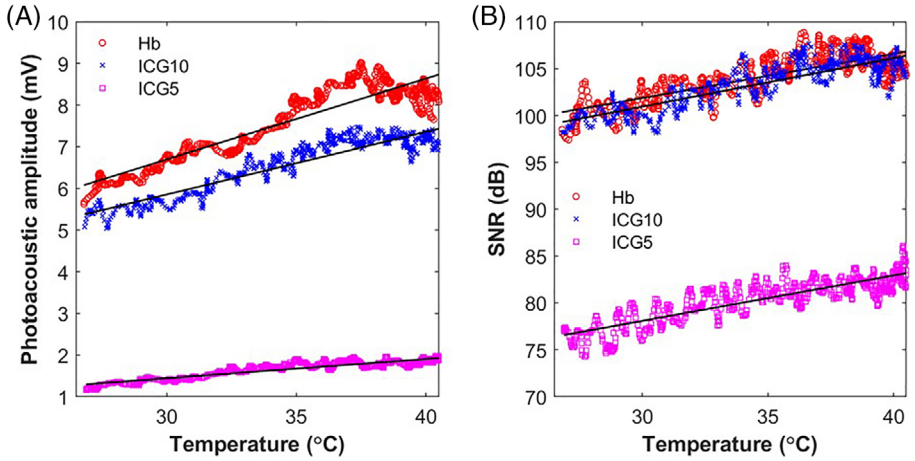

FIGURE 5 (A) Photoacoustic amplitude of three tubes containing Hb, ICG10 and ICG5, respectively, as temperature rises. Note that noise does not increase much as temperature rises (results not shown). (B) SNR of the three tubes as temperature rises. Black lines are linear fits to experimental data

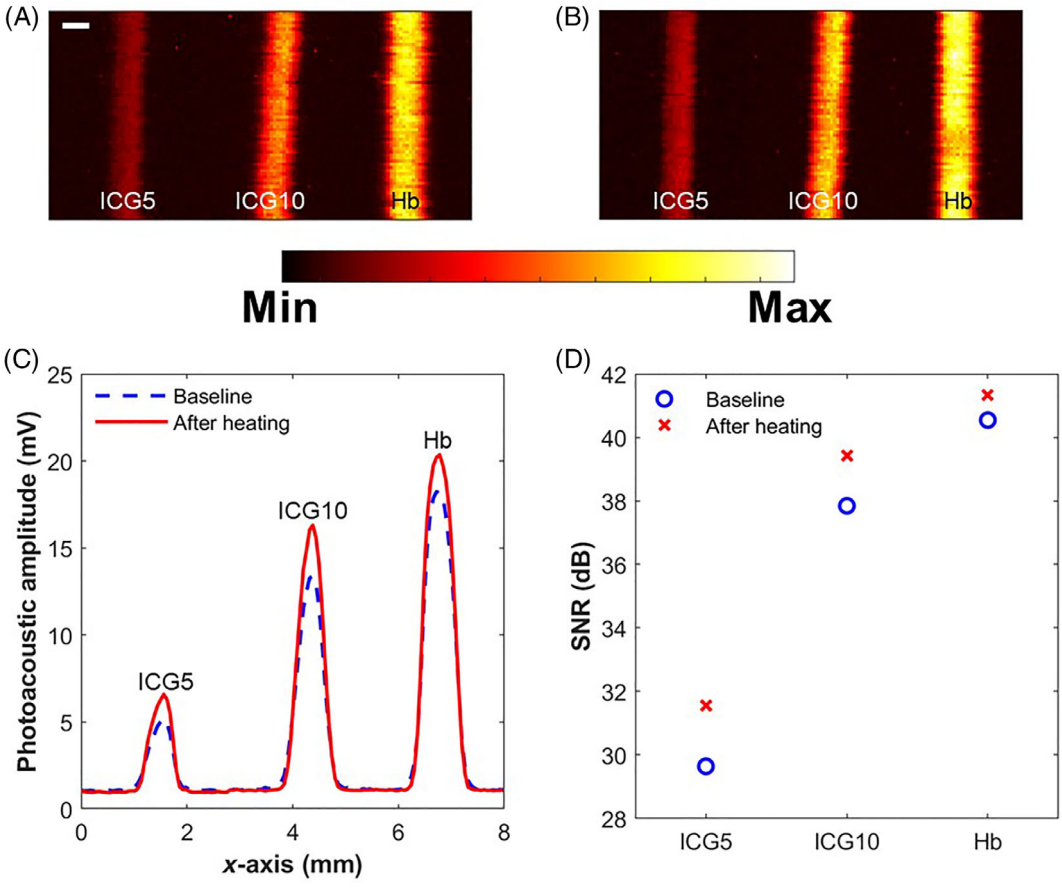

FIGURE 6 (A,B) AR-PAM of Hb (160 mg/mL), ICG10 and ICG5 in tubes at baseline temperature of 37°C (A) and at increased temperature of 41°C (B). The color map is for photoacoustic amplitude. Scale bar: 500 μm. (C) The 1D profiles of averaged photoacoustic amplitude along the horizontal line in (A) and (B) at the baseline temperature and after heating. (d) SNR calculated from (A) and (B) at the baseline temperature and after heating

For photoacoustic images acquired by AR-PAM and OR-PAM, photoacoustic A-line signals were first processed by a matched filter, and then, maximum amplitude projection (MAP) along the axial direction was applied to the 3D data to obtain 2D MAP images.

3 | RESULTS

3.1 | Nonlinear photoacoustic effect through longitudinal monitoring

Figure 4 shows photoacoustic amplitude and differential photoacoustic amplitude of porcine muscle and fat as temperature increases. In Figure 4A,B, as temperature increases, similar trends between the simulation and experimental results are observed for both photoacoustic amplitude (Figure 4A) and differential photoacoustic amplitude (Figure 4B). Specifically, photoacoustic amplitude of porcine muscle increases with temperature, while that of porcine fat slightly decreases with temperature. The opposite slopes of the curves in Figure 4A can be utilized to differentiate between porcine muscle and fat. Besides, the differential photoacoustic amplitude, reflecting the contrast between the two absorbers, increases from 6.4 mV (the minimum) to 34.9 mV (the maximum). The ~5.5 times enhancement in experiment is similar to the ~5 times enhancement in simulation mentioned previously (Section 2.1).

Figure 5 shows the results from three capillary tubes containing hemoglobin solution (Hb), ICG of 10 mg/mL (ICG10) and ICG of 5 mg/mL (ICG5). In Figure 5A, photoacoustic amplitude of Hb, ICG10 and ICG5 increases as temperature increases. Besides, in Figure 5B, SNR of the three absorbers increases as temperature increases, suggesting that noise does not increase much compared with photoacoustic amplitude for the tube samples.

Therefore, we experimentally confirmed that our approach is applicable for (a) enhancing photoacoustic contrast of different absorbers with different thermoacoustic properties and (b) enhancing photoacoustic amplitude and SNR of the tube samples.

3.2 | In vitro imaging

As mentioned in Section 2.6, the in vitro study was conducted to show the imaging capability of the proposed approach. The samples used in Figure 5 were also used

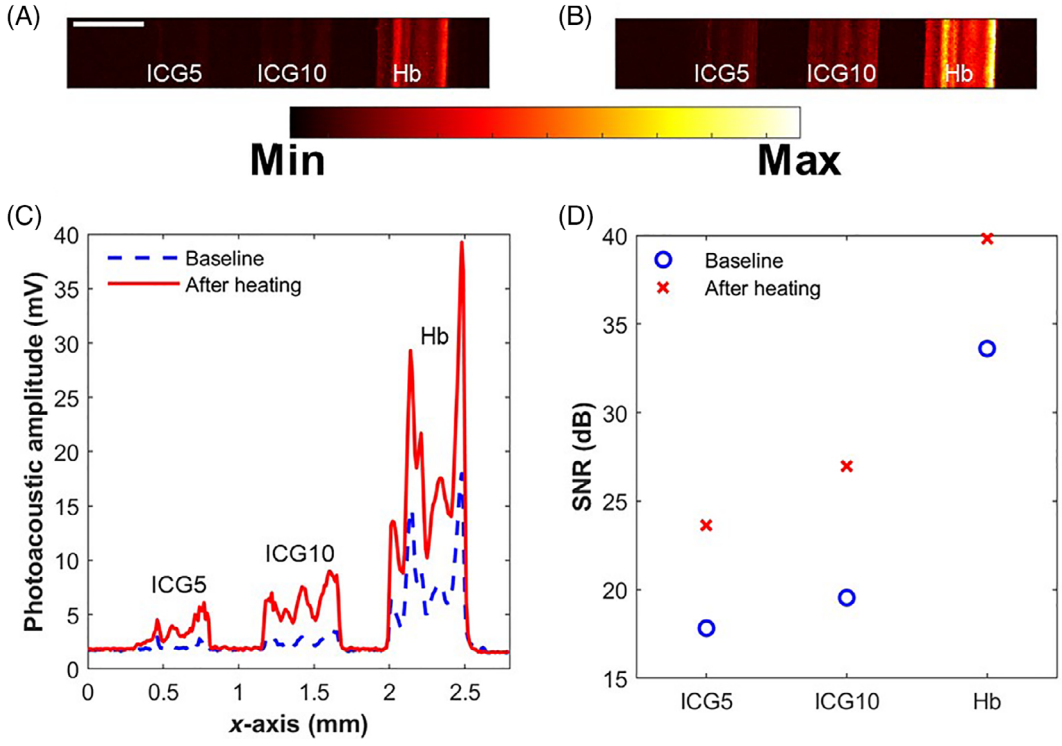

FIGURE 7 (A,B) OR-PAM of Hb (sheep blood), ICG10 and ICG5 in tubes at baseline temperature of 26°C (A) and at increased temperature of 32°C (B). The color map is for photoacoustic amplitude. Scale bar: 500 μm. (C) The 1D profiles of averaged photoacoustic amplitude along the horizontal line in (A) and (B) at the baseline temperature and after heating. (d) SNR calculated from (A) and (B) at the baseline temperature and after heating

here. Figure 6A,B shows AR-PAM images of Hb, ICG10 and ICG5 in tubes at baseline temperature and after IR lamp heating, respectively. Figure 6C shows 1D profiles of averaged photoacoustic amplitude along the horizontal line in Figure 6A,B. The averaged photoacoustic amplitude is obtained by calculating the average of photoacoustic amplitude along the vertical direction in Figure 6A,B. Figure 6C shows enhancement of averaged photoacoustic amplitude of the three samples after heating. Besides, Figure 6D shows SNR of the three samples increases after heating. As can be seen, Figure 6C,D are consistent with the longitudinal measurement result (Figure 5) that the photoacoustic amplitude and SNR of the three samples increase after heating.

Figure 7 shows the results acquired by OR-PAM. Overall, the results in Figure 7 are similar to Figure 6, showing that our approach can be applied based on OR-PAM as well.

4 | DISCUSSION AND CONCLUSIONS

Our proposed approach offers advantages in (a) enhancing photoacoustic contrast of different absorbers with different temperature-dependent Grüneisen coefficients (as demonstrated in the porcine tissue sample) and (b) enhancing photoacoustic amplitude and SNR of absorbers with the increase of Grüneisen coefficient with increased temperature (as demonstrated in the in vitro sample). Notably, for the former, one potential application would be differentiation of tumor and normal tissue based on the fact that tumor tissue tends to have lower lipid contents and higher water contents than normal tissue (i.e., utilizing different temperature-dependent Grüneisen coefficients between tumor and normal tissue) [36, 37].

It was reported that exposure of the skin at temperature of 43°C for less than 8 hours is not harmful [18]. In our ex vivo and in vitro demonstration, the temperature used is below 41°C and the time required for IR lamp heating is less than 8 hours. Thus, this suggests that safety may be ensured when applying our technique to in vivo and even clinical applications, although additional studies are required.

The speed of our approach is currently limited by PAM imaging speed and the steady heating procedure. For example, for the demonstration of in vitro imaging in Figure 7 using the setup in Figure 3B, it took a few minutes to acquire the OR-PAM image and another few minutes for the steady heating procedure (from 26°C to 32°C). The OR-PAM imaging speed can be boosted by using a pulsed laser with higher PRF. Besides, the steady heating procedure can be further expedited by heating a smaller region with a more focused IR light. Further optimization of the speed of our scheme could improve temporal resolution and even enable dynamic observation of nonlinear PAM.

In our demonstration, photoacoustic signals or images were acquired at different temperature, which was measured and monitored by placing the thermistor in the water tank (Figure 3). However, for in vivo and clinical applications, typically no water tank is used. The temperature measurement and monitoring of target tissue are required, which is also important to achieve precise and stable control of tissue temperature. To this end, one can employ a feedback control method to automatically adjust the IR lamp heating by monitoring the subsurface tissue temperature using a needle thermocouple or the deep tissue temperature using a high-intensity focused ultrasound (HIFU)-based technique [38, 39].

In Figures 5–7, photoacoustic signals of ICG were excited at laser wavelength of 532 nm because the pulsed laser at this wavelength is easily accessible. Nonlinear PAM of ICG can be conducted using its optimal absorption wavelength range (700–900 nm) for photoacoustic excitation [40], which enables high SNR at low excitation fluence and thus facilitates clinical applications of our approach. It is also worth noting that photoacoustic amplitude (or SNR) does not change linearly with the ICG concentration (e.g., ICG10 and ICG5) in Figures 5–7. This may be because of the nonlinear dependence of the optical properties of ICG on its concentration [41, 42]. Overall, in our demonstration, we observed enhancement of photoacoustic amplitude and SNR for ICG with two different concentrations.

Although PAI utilizing the steady heating mechanism was reported [11, 16, 17], different heating lasers were required depending on the absorption characteristics of sample [11], and only simple 1D imaging with low resolution was demonstrated [16, 17]. By contrast, in this work, IR lamp is cost-effective and imaging using AR-PAM and OR-PAM systems with different resolution is demonstrated.

In conclusion, we demonstrated a low-cost and simple approach for nonlinear PAM relying on steady heating. Compared with existing nonlinear PAM techniques, our approach employing an IR lamp is cost-effective and simple to realize sample heating. Because of heating by the IR lamp, various samples can be heated. By investigating a few samples, we experimentally verified the wide applicability of the proposed approach. By contrast, when heating using lasers, only samples with corresponding absorption wavelength can be used. Our work may find new opportunities for nonlinear PAM in biomedical applications.

ACKNOWLEDGMENTS

This work was supported by National Natural Science Foundation of China (NSFC) (61775134).

CONFLICT OF INTEREST

The authors declare no financial or commercial conflict of interest.

AUTHOR CONTRIBUTION

Myeongsu Seong: Conceptualization of the work and data analyses, performed simulations, developed AR-PAM system, performed experiments and wrote the original draft, developed OR-PAM probe and developed OR-PAM system. **Wenzhao Yang:** Developed OR-PAM probe and developed OR-PAM system. **Yujie Han:** Prepared samples. **Jiasheng Zhou:** Developed OR-PAM probe and developed OR-PAM system. **Lili Jing:** Prepared samples. **Sung-Liang Chen:** Conceptualization of the work and data analyses, supervised the study. All of the authors confirmed the manuscript before submission.

DATA AVAILABILITY STATEMENT

The data that support the findings of this study are available from the corresponding author upon reasonable request.

ORCID

Myeongsu Seong https://orcid.org/0000-0002-3472-8062
Sung-Liang Chen https://orcid.org/0000-0002-0572-5110

REFERENCES

[1] L. V. Wang, J. Yao, *Nat. Methods* **2016**, *13*, 627. https://doi.org/10.1038/nmeth.3925.
[2] J. Yao, L. V. Wang, *Photoacoustics* **2014**, *2*, 87. https://doi.org/10.1016/j.pacs.2014.04.002.
[3] M. Seong, S.-L. Chen, *Sci. China Life Sci.* **2020**, *63*, 1798. https://doi.org/10.1007/s11427-019-1628-7.
[4] L. Wang, C. Zhang, L. V. Wang, *Phys. Rev. Lett.* **2014**, *113*, 174301. https://doi.org/10.1103/PhysRevLett.113.266101.
[5] J. Ma, J. Shi, P. Hai, Y. Zhou, L. V. Wang, *J. Biomed. Opt.* **2016**, *21*, 066005. https://doi.org/10.1117/1.JBO.21.6.066005.
[6] X. Liu, T. T. W. Wong, J. Shi, J. Ma, Q. Yang, L. V. Wang, *Opt. Lett.* **2018**, *43*, 947, https://doi.org/10.1364/OL.43.000947.
[7] J. Shi, C. Li, H. Mao, Y. Ren, Z.-C. Luo, A. Rosenthal, K. K. Y. Wong, *Opt. Lett.* **2020**, *45*, 3268. https://doi.org/10.1364/OL.393780.
[8] F. Gao, X. Feng, R. Zhang, S. Liu, R. Ding, R. Kishor, Y. Zheng, *Sci. Rep.* **2017**, *7*, 626.
[9] H. Lan, T. Duan, D. Jiang, H. Zhong, M. Zhou, F. Gao, *IEEE Sensors J.* **2019**, *19*, 5559. https://doi.org/10.1109/JSEN.2019.2902849.
[10] T. Duan, H. Lan, H. Zhong, M. Zhou, R. Zhang, F. Gao, *Opt. Lett.* **2018**, *43*, 5611, https://doi.org/10.1364/OL.43.005611.
[11] A. Thomas, S. Paul, J. Mitra, M. S. Singh, *Sensors* **2021**, *21*, 1190. https://doi.org/10.3390/s21041190.
[12] F. Gao, X. Feng, Y. Zheng, *Appl. Phys. Lett.* **2014**, *104*, 213701.
[13] Y. Yamaoka, M. Nambu, T. Takamatsu, *Opt. Express* **2011**, *19*, 13365. https://doi.org/10.1364/OE.19.013365.
[14] Z. Zhang, Y. Shi, S. Yang, D. Xing, *Opt. Lett.* **2018**, *43*, 2336. https://doi.org/10.1364/OL.43.002336.
[15] O. Simandoux, A. Prost, J. Gateau, E. Bossy, *Photoacoustics* **2015**, *3*, 20. https://doi.org/10.1016/j.pacs.2014.12.002.
[16] W. Wang, A. Mandelis, *J. Biomed. Opt.* **2016**, *21*, 066018. https://doi.org/10.1117/1.JBO.21.9.096010.
[17] W. Wang, A. Mandelis, *Int. J. Thermophys.* **2016**, *37*, 74.
[18] W. Wang, A. Mandelis, *Biomed. Opt. Express* **2014**, *5*, 2785. https://doi.org/10.1364/BOE.5.002785.
[19] I. V. Larina, K. V. Larin, R. O. Esenaliev, *J. Phys. D: Appl. Phys.* **2005**, *38*, 2633. https://doi.org/10.1088/0022-3727/38/15/015.
[20] B. E. Treeby, B. T. Cox, *J. Biomed. Opt.* **2010**, *15*, 21314.
[21] V. K. Nagarajan, B. Yu, *Lasers Surg. Med.* **2016**, *48*, 686. https://doi.org/10.1002/lsm.22541.
[22] K. M. Sørensen, S. B. Engelsen, *J. Near Infrared Spectrosc.* **2017**, *25*, 45. https://doi.org/10.1177/0967033516685548.
[23] R. L. P. van Veen, H. J. C. M. Sterenborg, A. Pifferi, A. Torricelli, R. Cubeddu, in Biomed. Top. Meet., OSA, Miami Beach, FL, **2004**, p. SF4.
[24] R. M. Pope, E. S. Fry, *Appl. Optics* **1997**, *36*, 8710. https://doi.org/10.1364/AO.36.008710.
[25] S. Prahl, S. Jacques, https://omlc.org/ (accessed: September 2020). https://doi.org/10.1101/2021.12.09.21267423.
[26] T. C. Polachini, L. F. L. Betiol, M. G. Bastos, V. R. N. Telis, A. C. de Souza, J. Telis-Romero, *Can. J. Chem. Eng.* **2016**, *94*, 988. https://doi.org/10.1002/cjce.22468.
[27] B. Fricke, B. Becker, *HVAC&R Res.* **2001**, *7*, 311. https://doi.org/10.1080/10789669.2001.10391278.
[28] S. A. López-Haro, M. I. Gutiérrez, A. Vera, L. Leija, *J. Med. Ultrason.* **2015**, *42*, 489. https://doi.org/10.1007/s10396-015-0643-3.
[29] W. Wang, *Signal Strength and SNR Enhancement Techniques for Frequency Domain Photoacoustic Radar Imaging*, University of Toronto, Canada **2016**.
[30] G. S. Kell, *J. Chem. Eng. Data* **1975**, *20*, 97. https://doi.org/10.1021/je60064a005.
[31] N. Bilaniuk, G. S. K. Wong, *J. Acoust. Soc. Am.* **1993**, *93*, 1609.
[32] D. Cai, Z. Li, Y. Li, Z. Guo, S.-L. Chen, *Opt. Express* **2017**, *25*, 1421. https://doi.org/10.1364/OE.25.001421.
[33] C. Yeh, B. Soetikno, S. Hu, K. I. Maslov, L. V. Wang, *J. Biomed. Opt.* **2014**, *19*, 096011. https://doi.org/10.1117/1.JBO.19.9.096011.
[34] Z. Guo, Y. Li, S.-L. Chen, *Opt. Lett.* **2018**, *43*, 1119. https://doi.org/10.1364/OL.43.001119.
[35] Z. Ye, P. K. Srivastava, Y. Xu, W. Wang, L. Jing, S.-L. Chen, C.-C. Tu, *ACS Appl. Nano Mater.* **2019**, *2*, 7577. https://doi.org/10.1021/acsanm.9b01682.
[36] J. Wang, B. W. Pogue, S. Jiang, K. D. Paulsen, *Opt. Lett.* **2010**, *35*, 82. https://doi.org/10.1364/OL.35.000082.
[37] A. Cerussi, N. Shah, D. Hsiang, A. Durkin, J. Butler, B. J. Tromberg, *J. Biomed. Opt.* **2006**, *11*, 044005. https://doi.org/10.1117/1.2337546.
[38] N. T. Sanghvi, W.-H. Chen, R. Carlson, C. Weis, R. Seip, T. Uchida, M. Marberger, *J. Ther. Ultrasound.* **2017**, *5*, 24.

[39] A. Worthington, P. Peng, K. Rod, V. Bril, J. Tavakkoli, *IEEE J. Transl. Eng. Health Med.* **2016**, *4*, 1. https://doi.org/10.1109/JTEHM.2016.2581811.
[40] H. Wang, X. Li, B. W.-C. Tse, H. Yang, C. A. Thorling, Y. Liu, M. Touraud, J. B. Chouane, X. Liu, M. S. Roberts, X. Liang, *Theranostics* **2018**, *8*, 1227. https://doi.org/10.7150/thno.22872.
[41] A. Fernandez-Fernandez, R. Manchanda, T. Lei, D. A. Carvajal, Y. Tang, S. Z. R. Kazmi, A. J. McGoron, *Mol. Imaging* **2012**, *11*, 99. https://doi.org/10.2310/7290.2011.00031.
[42] V. Saxena, M. Sadoqi, J. Shao, *J. Pharm. Sci.* **2003**, *92*, 2090. https://doi.org/10.1002/jps.10470.

How to cite this article: M. Seong, W. Yang, Y. Han, J. Zhou, L. Jing, S.-L. Chen, *J. Biophotonics* **2022**, *15*(4), e202100301. https://doi.org/10.1002/jbio.202100301